Macromolecules

Article

pubs.acs.org/Macromolecules

Influence of Tie and Loop Molecules on the Mechanical Properties of Lamellar Block Copolymers

Ali Makke,[†,§] Olivier Lame,*[,†] Michel Perez,[†] and Jean-Louis Barrat[‡]

[†]Université de Lyon, INSA Lyon, MATEIS, UMR CNRS 5510, F69621 Villeurbanne, France

[‡]Université Joseph-Fourier, Grenoble, LIPhy, UMR CNRS 5588, Grenoble, France

[§]Université de Lyon, Université Lyon I, LPMCN, UMR CNRS 5586, F69622 Villeurbanne, France

ABSTRACT: We use coarse-grained molecular dynamics simulation to study the influence of molecular architecture and conformations on the mechanical response of lamellar nanostructured polymers. For this purpose, a recently developed generation method (radical like polymerization method) has been optimized to generate lamellar triblock copolymer samples with alternate glassy and rubbery stacks. Several systems, with various rate of *loop* (both ends of the chain are in the same glassy block), *cilia* (cut triblock, effectively a diblock chain) and *tie molecules (TMs)* (chain that bridges two subsequent glassy blocks through the intermediate rubbery block) were generated. Uniaxial tensile tests were performed, the tensile strain being applied in the normal direction of the lamellae. This situation can be understood as a simple way of mimicking the deformation of the equatorial stack in semicrystalline polymers, with the "hard" phase being the glassy (rather than crystalline) one. The resulting constitutive laws reveal the key role of the tie molecules in the transmission of stress between glassy blocks. Decreasing the amount of tie molecules with respect to cilia chain leads to a decrease in the entanglement density, which affects the yield and the strain hardening behavior. It is also demonstrated that loop chains play the exact same role as tie molecules because they are strongly entangled.

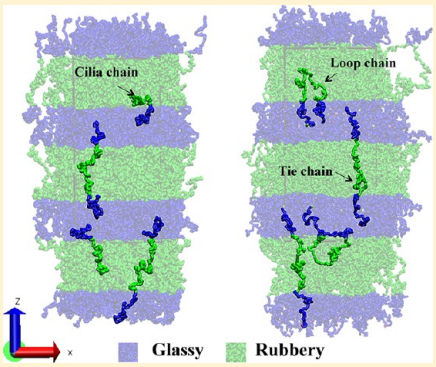

INTRODUCTION

Nanostructured polymers such as semicrystalline polymers, or block copolymers are used in a broad range of applications. Lamellar, stacked structures exist for both semicrystalline polymers and block copolymers. The mechanical response of such systems are based on the same concepts, whether the stack alternates glassy−rubbery or crystalline−rubbery phases, Lamellar semicrystalline systems have been widely studied, and their mechanical properties are globally well described.[1−6] However, the link between their microstructure and their molecular topology remains only qualitative, or even unclear. In particular, the question of stress transmission between hard and soft phases during deformation is of prior interest. This point has been mainly addressed for semicrystalline polymer, and it has been shown that the visco-elastic deformation is essentially governed by the amorphous (rubber) phase properties[7−11] until relatively high strains where crystallite start to undergo shear defomations. Therefore, the molecular topology of the amorphous phase, and the associated parameters such as the molecular weight and the entanglements density, are decisive parameters that have been shown to influence the plastic behavior of semicrystalline polymers such as polyethylene.[1,2,12,13] Among all the possible molecular topology, tie molecules (TMs), linking two adjacent crystallites, are supposed to contribute most effectively to the mechanical behavior of semicrystalline polymers.[5,14] It is indeed likely that chains that link together two adjacent crystallites (hard phase) should play a crucial role on stress transmission and more generally on the global mechanical behavior. Despite several studies on this subject,[13,15,16] it is experimentally impossible to (i) quantify the TM density and (ii) to evaluate their exact contribution to the global mechanical behavior. The concentration of stress transmitters has been roughly evaluated using macroscopic indicators such as the strain hardening measured on a stress/strain curve. (see refs 17−19, for example). However, because of their macroscopic and indirect nature, the reliability of such indicators can be questioned. Finally, it is almost impossible to precisely state what kind of molecules could be described as a stress transmitter.

A similar challenge was also addressed experimentally for lamellar block copolymers. The role of the molecular architecture has been investigated and a clear transition from brittle to ductile failure was observed when a sufficient amount of pentablock chains is mixed with triblock chains,[20] i.e., when the mechanical bridging is enhanced via longer chains. As for semicrystalline polymers, a quantitative analysis of these experiments is extremely difficult and very few numerical studies have been performed concerning the TMs.

On the modeling side, Bonten et al.[16] have demonstrated trough a finite element calculation that the density of TMs could be determinant for the value of the transmitted force. On a related topic, Sides et al.[21] have studied the tensile strain response of a polymer melt confined between two rigid walls using coarse-

Received: June 26, 2012
Revised: September 13, 2012

dx.doi.org/10.1021/ma301286y | *Macromolecules* XXXX, XXX, XXX−XXX

grained molecular dynamics simulation. They found that the global response of the sample is sensitively dependent on the density of the chains end-tethered to the wall. On semicrystalline polymers, Monasse et al. have studied the local mechanical behavior of semicrystalline polyethylene model using atomistic molecular dynamics. These studies have revealed the role of TMs on the damage of the crystalline lamellae.[22] Similarly, Lee et al. showed using Monte Carlo and molecular dynamics that melting and cavitation occur during deformation of a model semicrystalline polyethylene.[23] In the latter study, however, the specific role of TMs was not discussed. Coarse-grained molecular simulations appears to be a particularly suitable tool to explore the issue, as the chain topology can be easily described and high deformation rate can be reached for relatively short computation time.

In this paper, the effect of cilia (diblock chains with a dangling end in the soft phase), tie, and loop molecules on the mechanical behavior of lamellar, triblock copolymers is investigated using coarse-grained molecular dynamics simulations. Our investigation is restricted to lamellar block copolymers with glassy and rubberry lamellae, as the generation of semicrystalline polymers is more complex. However, considering these systems as a hard/soft lamellar stack, the results could be also of interest (at least at a qualitative level) for semicrystalline systems. The mechanical response has been evaluated in tensile conditions when the tensile stress is perpendicular to the length of the lamellae. This choice of the mechanical coupling corresponds to the geometry of the equatorial stack for semicrystalline polymers. Several systems have then been numerically produced with various fractions of tie and loop molecules. The relation between mechanical behavior and molecular topology is compared to results of the literature.

SIMULATION TECHNIQUES AND SAMPLE GENERATION

Model. Molecular dynamics (MD) simulations were carried out for a well established coarse-grained model,[24] in which the polymer is treated as a chain of N beads, which we refer to as monomers, of mass $m = 1$ connected by a spring to form a linear chain. The beads interact with a classical Lennard-Jones (LJ) interaction:

$$U_{\mathrm{LJ}}^{\alpha\beta}(r) = \begin{cases} 4\varepsilon_{\alpha\beta}\left[\left(\frac{\sigma_{\alpha\beta}}{r}\right)^{12} - \left(\frac{\sigma_{\alpha\beta}}{r}\right)^{6}\right], & r \le r_c \\ 0, & r \ge r_c \end{cases} \quad (1)$$

where the cutoff distance $r_c = 2.5\sigma$. α and β represent the chemical species (*i.e.*, A, B) In addition to eq 1, adjacent monomers along the chains are coupled through the well-known anharmonic finite extensible nonlinear elastic potential (FENE):

$$U_{\mathrm{FENE}}(r) = \begin{cases} -0.5kR_0^{\,2}\ln\left[1 - \left(\frac{r}{R_0}\right)^2\right], & r \le R_0 \\ \infty, & r > R_0 \end{cases} \quad (2)$$

The parameters are identical to those given in Kremer et al.,[24] namely $k = 30\varepsilon/\sigma^2$ and $R_0 = 1.5\sigma$, chosen so that unphysical bond crossings and chain breaking are avoided. All quantities will be expressed in terms of length σ, energy ε, pressure ε/σ^3 and time $\tau = ((m\sigma^2)/\varepsilon)^{1/2}$.

Newton's equations of motion are integrated with the velocity Verlet method and a time step $\Delta t = 0.006\tau$. Periodic simulation cells containing $M = 430 \pm 3$ chains of size $N = 200$ beads were used with a Nosé-Hoover barostat, i.e. in the NPT ensemble. An anisotropic barostat with $P_x = P_y = P_z = 0$ is used in the equilibration, leading to a tetragonal simulation box before running the tensile test.

The final box dimensions are not identical for all samples, as they depend on several thermodynamical factors (temperature, LJ energy parameters, ...) and molecular architectures.

Sample Generation. The generation of segregated block copolymers is delicate, since each chain belongs to two or more blocks with different properties. Conventional methods like "fast push off" or double bridging hybrid[25] can not be used in this case. Our samples have been generated using the "Radical-Like Polymerization" (RLP) method,[26] where the polymerization takes place in a LJ monomer liquid bath, transforming it to a polymer or copolymer melt.

Basic Concepts. The generation of the sample is performed in three stages. In the **nucleation stage**, a number of beads are chosen from the solvent to behave as radicals. Each radical is allowed to connect to one of the available nearest neighbors with a strong covalent bond. The radical sites are then transferred to the new connected beads, allowing the chains to grow. Between two **growth stages**, the entire system is relaxed during 100 MD steps. The polymerization propagates until all chains reach their target length. When the generation is achieved, residual single beads are removed and the system is relaxed for 10^7 MD steps in NPT ensemble at $k_BT = 1\varepsilon$ and $P = 0$ to reach an equilibrium state. This last step is the **finalization step** .

Generation Method. The basic version of The RLP method has been optimized to generate periodic triblock copolymer samples $A_1B_1A_2B_2$ with four interfaces parallel to the (xy) plane. This size is needed in order to avoid unphysical folding of the triblock chains due to periodic boundary conditions along the z diretion: here a triblock chain can actually bridge two physically distinct lamellae.

The generation is performed as follows. Starting from a LJ liquid of monomers, the simulation box of size $L \times L \times L$ is equally divided into four distinct regions along the z direction: A_1, B_1, A_2, and B_2. Each region has a width of $L/4$ (Figure 1a)

1. Radical beads are chosen randomly in A_1 and A_2 regions only (Figure 1.b).
2. Growth is performed until chains reach the size $N/4$. Note that radicals are only allowed to combine with beads that are located in their own region (A_1 or A_2, see Figure 1c,d).
3. Radical of chains of length $N/4$ are then attracted to the nearest interface thanks to an additional sinusoidal potential.
4. Growth is then performed in the neighboring region (B_1 or B_2) until chains reach the size $3N/4$ (Figure 1e,f).
5. Radicals of chains of length $3N/4$ are then attracted to the appropriate interface thanks to another additional sinusoidal potential: either back to the initial region for loop chains or toward the third domain. (A_2 if the polymerization started from A_1 and *vice versa*) for TMs (see Figure 1g).
6. Chain growth finally occurs until chains reach size N and the polymerization is stopped when all chains reach the target length of N (Figure 1h).

Note that after each growth step, the system is relaxed 100 MD steps in NPT ensemble at $k_BT = 2\varepsilon$ and an isotropic compressive pressure $P = 0.5\varepsilon/\sigma^3$. It is also important to remark that the proportion of loop and tie chains is *a priori* fixed by the

dx.doi.org/10.1021/ma301286y | Macromolecules XXXX, XXX, XXX–XXX

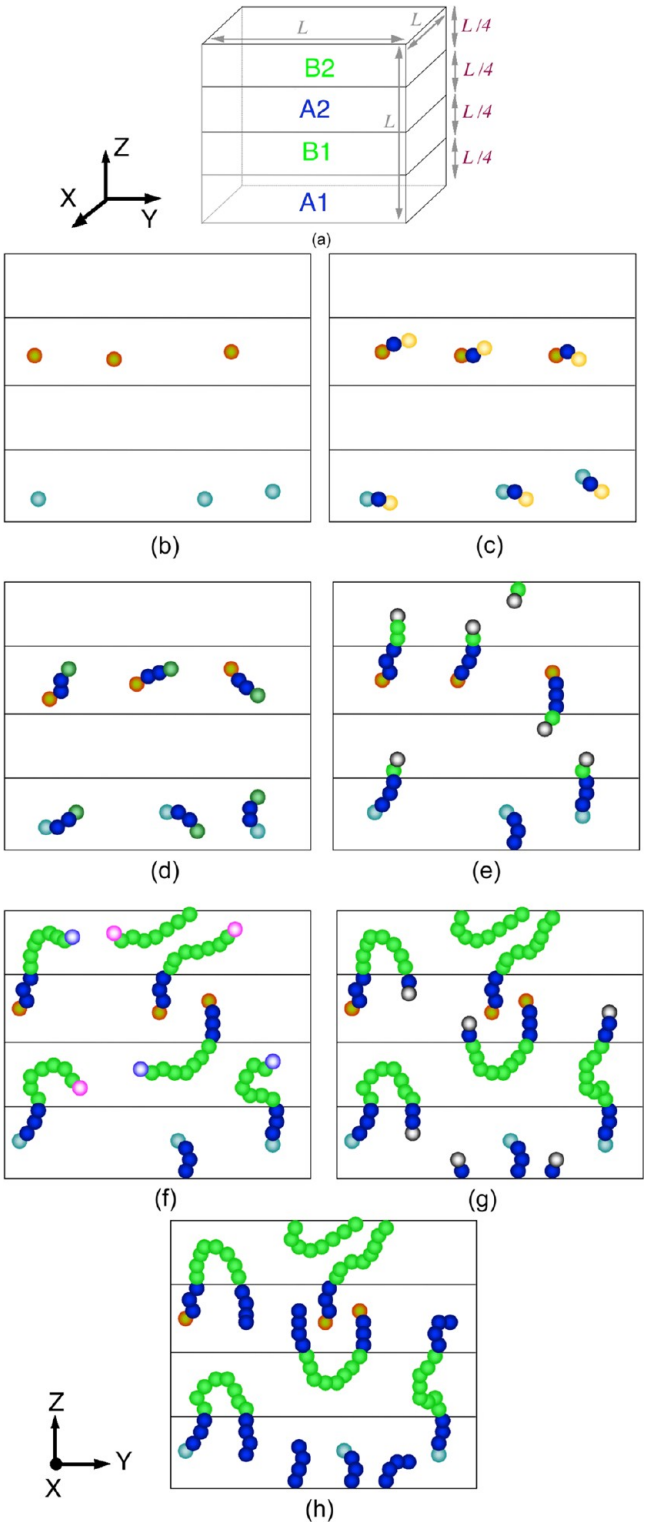

Figure 1. schematic representation showing the evolution of the generation procedure: (a) splitting of the simulation box, (b) nucleation stage, (c) growth within A and B domains, (d) migration of radicals toward nearest interface, (e) growth within B_1 and B_2, (f) migration of radical toward appropriate interface depending on chain type (loop or tie), (g) growth within A and C, (h) termination: the growth is stopped when the chains reach the requested length. The solvent is not shown in this figure.

generation procedure. Any equilibration procedure that would allow interconversion between the two conformations would be far too long, or involve melting the sample. This situation is also met in experiments, where the proportion of different conformations will in general result from a nonequilibrium process, rather than from equilibrium statistical physics considerations.

Finally, the resulting number densities are 1.06 σ^{-3}, 0.784 σ^{-3} and 0.907 $\sigma^{-3}$for glassy, rubbery and for the whole sample, respectively.

Generation Post Processing. Equilibration–Segregation. After the generation process, the remaining solvent is removed from the simulation box. The LJ interaction energies are adjusted to drive the segregation and the surface tension energy between blocks. In all cases of this study, the LJ energies are taken as follows: $\varepsilon_{AA} = 1\varepsilon$, $\varepsilon_{BB} = 0.2\varepsilon$ and $\varepsilon_{AB} = 0.35\varepsilon$ (this choice will be discussed later). The system is then relaxed 10^7 MD steps in NPT ensemble at $k_BT = 1\varepsilon$. All pressure components are maintained at zero ($P_x = P_y = P_z = 0$) using an **anisotropic** barostat, that allows the change in the box size in the three dimensions independently. The evolution of box lengths during the relaxation steps is measured. We found that all box dimensions reach steady state values after 10^7 MD steps, i.e., indicating that mechanical equilibrium between blocks is reached.

Along the relaxation steps, we have also checked the diffusion of the chains. Because of the lamellar structure of the sample, chains cannot diffuse in the normal direction of the lamellae (z direction). Therefore, the chain diffusion is measured only in the parallel direction (x and y). We found that the chains diffuse at least one time their own gyration radius in the parallel direction, indicating a good equilibration of the copolymer sample (for the prescribed proportion of loop and tie molecules).

Modifying the Chain Architecture. As described before, the used version of RLP method can only generate tie and loop molecules. Cilia chains were artificially created by cutting randomly a number of TMs for a given equilibrated sample without loop chains. Samples with different amounts of cilia chains have then been prepared in which TMs are cut right in their middle. The sample is finally relaxed 10^7 MD steps in order to well disperse the new created chain ends in B_1 and B_2 blocks.

Since cilia chains are randomly chosen from the TMs, the same number of cilia chains crosses each interface of the sample. Therefore, the chain ends are equally distributed between the two blocks B_1 and B_2 after the cutting. At the end of the generation and the post processing procedures several samples with various molecular architectures are then generated as shown in Figure 2.

In principle, each sample could contain a mixture of the three different types of chains. For the sake of simplicity, we limit our study to systems that are modified from the "ideal" situation (only TMs) by introducing either a finite fraction of loops, or a finite fraction of cilia.

To refer to a specific sample we use the nomenclature S_c^x for the sample with x% cilia and S_l^x, for the sample with x% loop chains. (e.g S_c^{60} designates a sample for which 60% of TM were cut). All samples that are studied in this paper are summarized in Table 1.

Choice of Temperature. To reproduce the behavior of a nanostructure formed by an alternate stacking of hard and soft phases, the temperature has to be chosen so that one phase is glassy while the other is rubbery. The glass transition temperature of each phase was identified by cooling the sample from $k_BT = 1\varepsilon$ where both phases are rubbery to $k_BT = 0.01\varepsilon$, where both phases are glassy (cooling rate: 1.6×10^{-4} $\varepsilon/(k_B\tau)$).Figure 3 shows the change of $\log(V)$ as a function of the

dx.doi.org/10.1021/ma301286y | *Macromolecules* XXXX, XXX, XXX–XXX

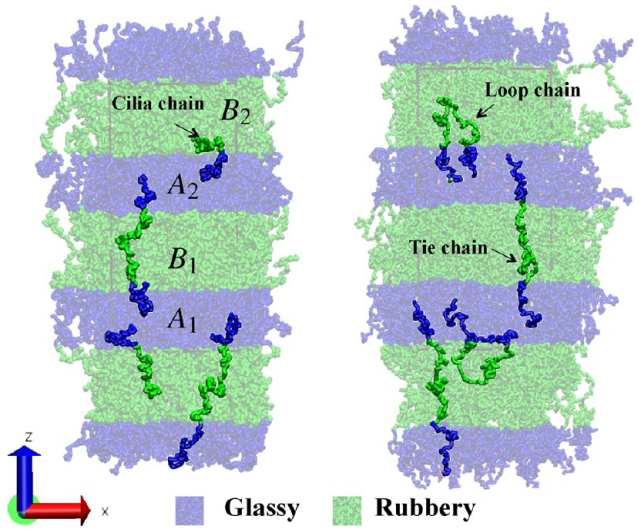

Figure 2. Two snapshots highlighting the different chain architectures in our triblock sample model: cilia, loop, and tie molecules (TMs). Samples may contain one or two of these types *e.g* cilia, loop and/or tie molecules. A_1 and A_2 are the glassy phases while B_1 and B_2 are the rubbery phases at $T = T_{test}$. The relevant interaction energies are $\varepsilon_{AA} = 1\varepsilon$, $\varepsilon_{BB} = 0.2\varepsilon$, and $\varepsilon_{AB} = 0.35\varepsilon$.

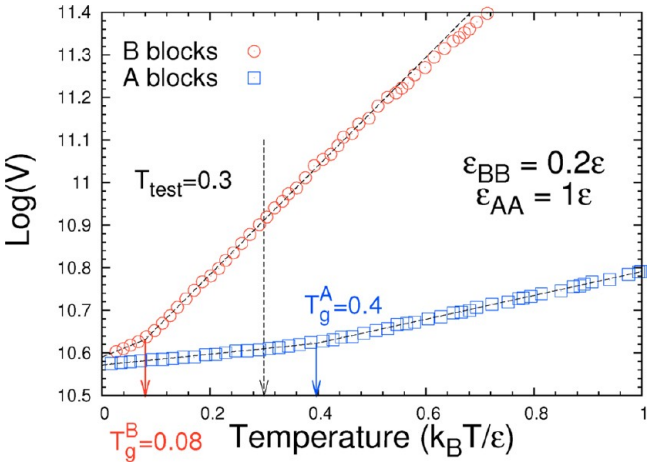

Figure 3. Glass transition of the two different phases are determined by monitoring the volume when cooling from $k_BT = 1\varepsilon$ to $k_BT = 0.001\varepsilon$ during 10^6 MD steps. The glass transition temperature T_g of each phase corresponds to the change in slope.

temperature, for each phase taken independently. Two linear (or quasi linear) regimes can be distinguished for each curve, the change of slope between these two regimes marks the glass transition of each phase. After the identification the glass transition temperature of each phase A and B, the tensile test temperature T_{test} is chosen in the middle of the interval between T_g^A and T_g^B. Thus, at T_{test}: phase A is the hard phase (in a glassy state at $T = T_{test}$) and phase B is the soft phase (in the rubbery state at $T = T_{test}$). Specifically, the temperature selected for our simulations is $k_BT = 0.3\varepsilon$. Note that at this temperature, the diffusion in the glassy hase is essentially zero on any practical time scale. Hence our samples are "frozen" in terms of chain diffusivity across interfaces,[27] unless a mechanical stress is applied.

Finally, the interaction energy ε_{AB} has to be specified. This parameter is important for the mechanical properties of the samples as it determines the surface tension and then the segregation between the two phases. A very low ε_{AB} leads to a compressible interface that favors the nucleation of cavities at relatively small strain, whereas a higher value may prevent the segregation by mixing both phases A and B during the relaxation stage. We choose a value $\varepsilon_{AB} = 0.35\varepsilon$, which corresponds to a strong segregation even at $k_BT = \varepsilon$, but preserves a good cohesion at the interface..

Tensile Test. In order to deform our samples, uniaxial homogeneous tensile conditions were employed.[28] The samples were subjected to a sequence of deformation-relaxation, composed of the following:

(i) a rescaling of the z dimension of the simulation box, whereas the two other dimensions are unchanged;

(ii) one MD step in the NVT ensemble for z axis and NPT ensemble for x and y axis (Nosé-Hover barostat $P_x = P_y = 0$). The temperature is maintained at $k_BT_{test} = 0.3\varepsilon$ by a Nosé−Hoover thermostat.

The deformation−relaxation sequence is such that the true initial strain rate is $\dot{\varepsilon}_{zz} = \dot{L}_z/L_z = 7.3 \times 10^{-5}\tau^{-1}$ (the time step is 0.006 τ). Typically, a stress−strain test requires 10^7 deformation−relaxation steps.

RESULTS

Description of a Typical Stress/Strain Curve. Figure 4a shows the stress/strain curve for the S_0^c sample, with only TMs. In order to correlate the mechanical behavior with the local deformation of blocks, the deformation of the glassy phase is plotted versus the global true strain (secondary y axis). The deformation of each rubbery block is also plotted versus the global true strain in the inset. The stress increases linearly in the elastic regime. As shown in the inset, only the rubbery blocks deform in this regime. The glassy blocks in this case behave as rigid grips that constrain the deformation of the rubbery blocks in the lateral directions. Therefore, the rubbery blocks are, effectively, submitted to triaxial stress conditions.

The stress drop observed after the elastic regime corresponds to cavitation in the soft blocks (see the snapshots in Figure 4b). The occurrence of the first cavitation event relaxes the tensile stress, but as deformation increases in block B_2, strain hardening starts to occur in this block. Then, cavitation occurs in the second block B_1 as it starts to deform, giving thus a fast increase in the local strain of block B_1. Until a true strain of 100%, the deformation is localized in the soft phase and the glassy phase is nearly undeformed. When the global deformation reaches 100%, the stress is high enough to trigger the plastic deformation of the hard phase leading to a strain hardening regime.

Table 1. Molecular Composition of the Samples That Are Used in This Study[a])

nomenclature and composition	$S_c^0 \equiv S_l^0$	S_c^{20}	S_c^{40}	S_c^{60}	S_c^{80}	S_c^{90}	S_c^{100}	S_l^{40}	S_l^{80}	S_l^{100}
% tie molecules (TMs)	100	80	60	40	20	10	0	60	20	0
% loop chains	0	0	0	0	0	0	0	40	80	100
% cilia	0	20	40	60	80	90	100	0	0	0

[a]Note that all of samples have the same LJ potential parameters $\varepsilon_{AA} = 1\varepsilon$, $\varepsilon_{BB} = 0.2\varepsilon$ and $\varepsilon_{AB} = 0.35\varepsilon$, and ($\sigma_{\alpha\beta} = 1\sigma$ for all phases.

dx.doi.org/10.1021/ma301286y | *Macromolecules* XXXX, XXX, XXX−XXX

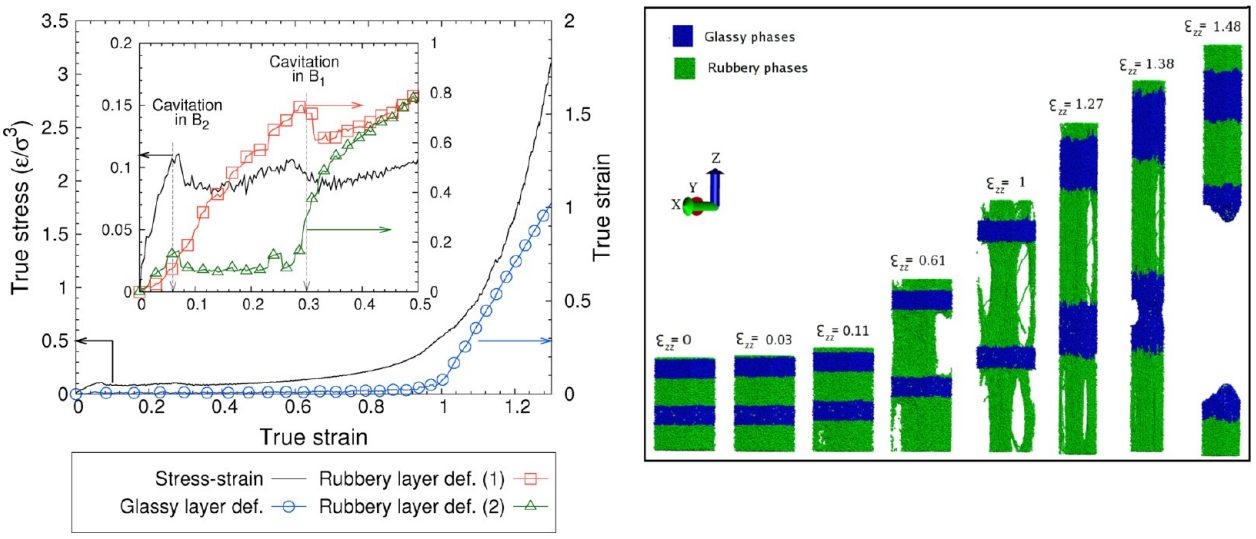

Figure 4. Left panel: stress/strain curves for the S_c^0 ("ideal") sample. The deformation of the glassy and rubbery phases is plotted versus the global true strain. The inset shows the small deformation part of the stress strain curve, and the deformation within each of the rubbery layers. Right, snapshots of the deformed lamellar stack taken at different levels of strain. It can be observed that cavitation (observed in the right panel) leads a stress drop (observed in the left panel). Moreover, the deformation of the hard phase is correlated with the hardening of the soft phase.

As in molecular simulations the strain rate is considerably higher than in experimental conditions, parameters for rubbery phase have been chosen so that it is extremely soft. Moreover, the lateral size of our sample is not large enough to allow fragmentation and plasticity mechanisms of the hard phase.

The cavitation of soft phase is therefore favored over plastic deformation of hard phase and, thus, appears before, which may not be the case in real conditions. This particular behavior is however encountered in specific cases for semicrystalline polymers,[29] even though it is strongly magnified in the present study.

Moreover, as the hard phase is not well entangled due to its short length (50 beads, lower than entanglement length), and as the rupture of covalent bonds is not allowed, the deformation of the glassy phase will align and disentangle the glassy chains, leading to the rupture of the weaker glassy phase. Despite of these numerical contingencies the comparison between the different systems remains perfectly valid.

Effect of the Molecular Topology on the Stress/Strain Curve. Figure 5 presents the mechanical behavior of several samples with different fractions of ciliae molecules. In the elastic regime all samples have roughly the same elastic modulus (see the inset). The yield stress increases slightly as the fraction of TMs increases. For these samples, the yield is due to the nucleation of cavities in the rubbery blocks. Then it appears that the rubber exhibit a better resistance to cavitation when the fraction of TMs is high. This result is qualitatively comparable to experimental observations made on semicrystalline polymers.[13,29] The stress drop at cavitation is more significant in the soft phases of samples with a small fraction of TMs. Again, this appears to be consistent with the literature reports that the plastic instability can be correlated to the fraction of TMs.[14,30]

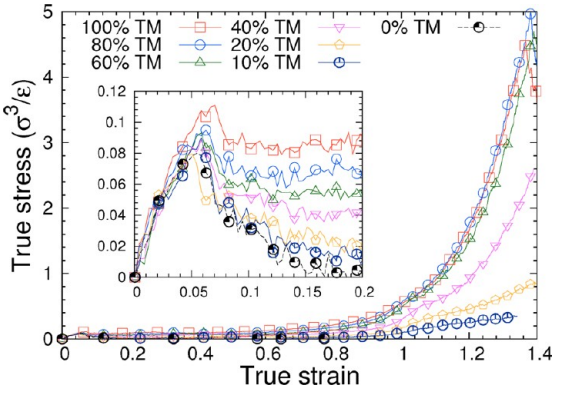

Figure 5. Comparison between the mechanical responses of several samples with different rates of cilia (cut molecules), the rest being tie molecules). Inset: zoom on the elastic and the yield parts of the curves.

Considering now the whole stress/strain curve, the stress supported at a given deformation is seen to be always an increasing function of the fraction of TMs. This is particularly significant in the hardening regime where the well-bridged samples exhibit a strong hardening slope, contrary to the weakly bridged samples. This result is consistent with the ideas actually present in literature for semicrystalline polymers: the fraction of TMs is indeed known to be essential at high deformation. Note that there is no significant difference between 0% and 40% of cilia chains in strain hardening. This observation leads to the conclusion that the stress is nearly completely transmitted with only 60% of TMs.

Role of Tie Molecules on Strain Hardening. In the hardening regime, semicrystalline polymers are often described as rubbers, with an entanglement density linked to the concentration of TMs.[31] Although this interpretation is oversimplified, it naturally leads to the definition of a hardening modulus using the usual formula for rubber elasticity:[32]

$$G = \frac{d\Sigma_{zz}}{d\left(\lambda^2 - \frac{1}{\lambda}\right)} \tag{3}$$

Here λ is the elongation and Σ_{zz} the stress measured in the tensile direction z.

The stress−strain curves have then been reanalyzed by plotting the stress versus λ^2-1/λ in order to determine the modulus G. Figure 6 shows the strain hardening modulus measured at two different strains: at $\varepsilon_{zz} = 0.88$, where only the

dx.doi.org/10.1021/ma301286y | Macromolecules XXXX, XXX, XXX−XXX

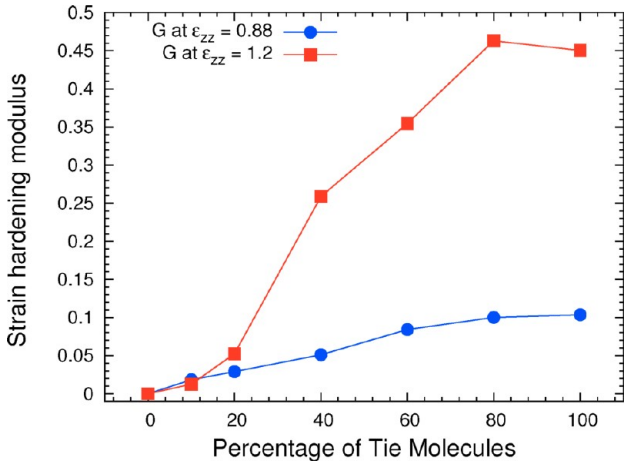

Figure 6. Instantaneous strain hardening modulus G of several samples with different rates of cilia molecules measured a true strain of 0.88 and 1.2 (samples are the same as in Figure 5).

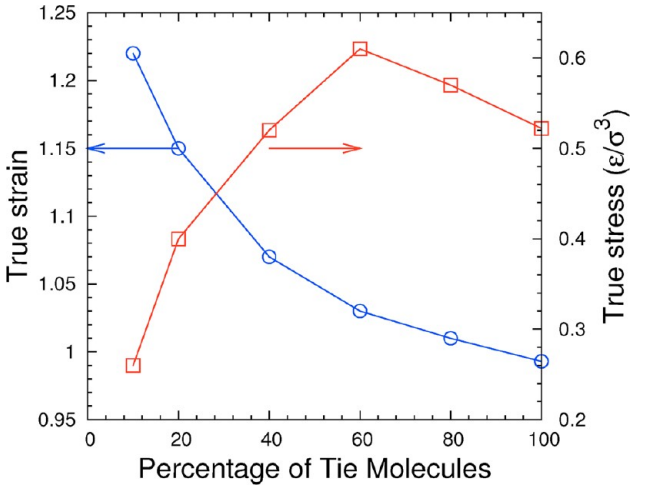

Figure 7. Influence of the tie molecules (TMs) on the transmission of stress between the hard phases. The blue (red) curve marked by circles (squares) shows the strain (stress) from which the hard phase starts to deform.

soft phase deforms significantly and at ε_{zz} = 1.2, where both phases deforms simultaneously. Note that the first condition is more frequently encountered in experimental cases.

At ε_{zz} = 0.88, the evolution of the modulus G appears to be quasi linear with the fraction of TMs up to 60%. In the classical rubbery theory, at a given temperature, the modulus is indeed considered to depend linearly with the entanglement density. This suggests that until 60%, the TM can be effectively considered as entanglements, as they induce an analogue mechanical effect, in agreement with Bartczak assumption.[31] After 60%, the hardening modulus saturates: probably because any additional TMs is useless from a mechanical point of view.

At ε_{zz} = 1.2, the evolution of the modulus G appears to strongly increase up to 80%. As the hardening is related to the plastic deformation of the glassy lamellae, this suggests that the fraction of the hard phase that is effectively concerned by the plastic deformation is essentially related to the fraction of stress transmitters, i.e., TM. Above 80%, it appears that the addition of extra stress transmitter does not mobilize more plasticity in the glassy phase. When the distance between stress transmitter crossing the interface becomes comparable to the distance between entanglements, adding more transmitters becomes effectively useless and the hardening modulus becomes the one of a pure glassy phase.

Role of Tie Molecules on Stress Transmission to Hard Phases. It is reported in the literature that TM plays a significant role on stress transmission between hard and soft phase. Again, this issue cannot be addressed quantitatively without molecular simulation. In Figure 7, we report the initiation of plastic deformation in the hard phase as a function of the percentage of TMs.

As the fraction of TMs increases, the stress to initiate plastic deformation in the hard phase increases. The more TMs, the less concentrated the stress is on the hard lamellae. This tendency has been also reported on semicrystalline polymer by Bonten et al.,[16] using finite element calculations. They demonstrated that the density of TMs is determinant on the stress concentration on the hard phase. Analogue results have been found on the initiation of plasticity of polyethylenes.[33] Similarly, Sides et al.[21] showed that weakly bridged systems damage by chain pullout in the hard phase.

The opposite tendency is observed for the strain at which plastic deformation is initiated in the hard phase. Indeed, as demonstrated above, the modulus of the soft phase increases with TMs rate. The yield stress of the hard phase is then reached at lower strain.

In order to interpret these results, the structure of copolymer blocks has been analyzed at the molecular scale, for a deformation beyond the onset of plasticity of the hard phase *i.e.* at a true strain of ε_{zz} = 1.2. Figure 8a shows snapshots of samples with TM concentration ranging from 100% to 10%. Depending on the amount of TM, two different scenarii for hard phase damage can be inferred: (i) at high TM concentration, the stress is homogeneously transmitted to the hard phase so that hard phase is itself homogeneously deformed; (ii) at low TM concentration, the stress is so concentrated that only a few chains are pulled out of the hard phase, so that the hard phase remains almost undeformed. Note that chain pull-out was mentioned by Sides et al.[21] and Monasse et al.[22] on particular systems, which did not allow homogeneous deformation of the hard phase.

Figure 8a shows the local density profile of the hard phase and permits the evaluation of both the thickness of the glassy lamellae and the width of the interface (region of intermediate density). First, this figure confirms the finding of Figure 8: high TM concentration leads to homogeneous deformation of hard phase (strong increase of glassy lamellae thickness) with a moderate broadening of the interface, whereas low TM concentration leads to quasi constant hard phase thickness ($\approx 20\sigma$) and sharp interface.

Note that intermediate TM concentration (around 40−60%) exhibit interesting results: the competition between homogeneous deformation and chain pull-out leads to the destabilization of the interface, visible on Figure 8 for 40% TM. This phenomenon could be the cause of the saturation observed in Figure 6.

Role of Loop Chains. Triblock chains that keep their integrity can adopt two different conformations, either TMs that will act as TMs, or loop chains with both ends belonging to the same hard lamella. Such loop chains could be considered as similar to a pair of ciliae, as they do not connect directly two different lamellae. They are however different from cilia, as no chain end lies in the rubber phase. In fact, two different configurations are possible for these chains. Either the loops anchored in one hard block are entangled with a loop anchored in

dx.doi.org/10.1021/ma301286y | *Macromolecules* XXXX, XXX, XXX−XXX

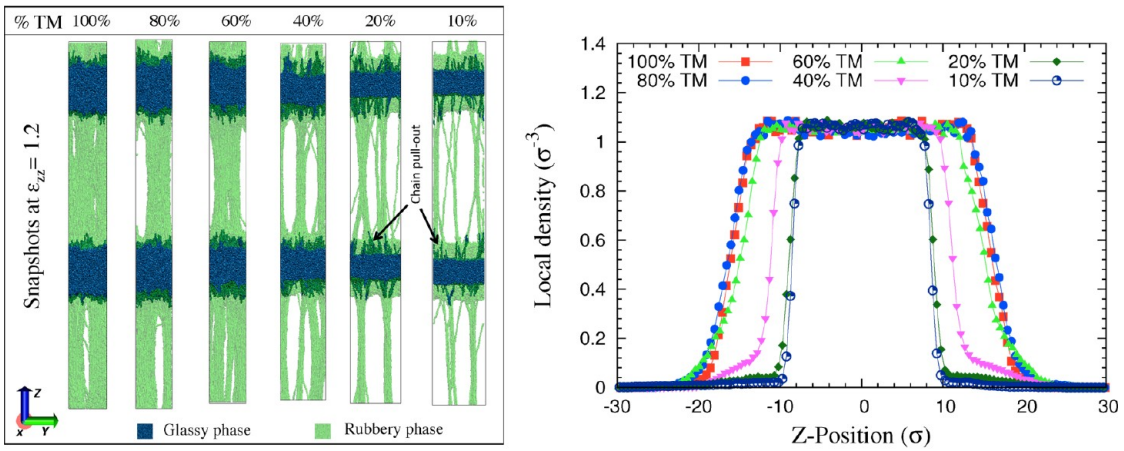

Figure 8. Samples deformed at ε_{zz} = 1.2 for 100% to 10% of tie molecules (TMs). (a) Snapshots (rubber, translucent green; glassy, blue). (b) Density profile of a glassy block (all curves were centered in the middle of the glassy block). Decreasing the TM concentration favors the chain pullout over the bulk deformation in the glassy blocks.

the second block or not. In other words, the mechanical influence of loop chains will depend on the possibility of separating the two hard blocks be separated without breaking them.

From an experimental point of view the two configurations are possible and depend on the chain length and probably on the process. The numerical process used here, tend to maintain the chain in a state close to the equilibrium during the preparation of the samples.[26] This method is probably the most realistic to simulate what would happen for real chains. Then, several samples with different amounts of loop chains were built as described in section (eq 2). The other chains remain TMs. Uniaxial tensile tests were applied and the test conditions are the same as previously described.

Figure 9 represents the constitutive laws of four systems with different fractions of loop/tie molecules. For the sake of comparison, a system with 20% of cilia and 80% of TMs is also represented on the same graph. It appears clearly that increasing the fraction of loop chains does not modify strongly the mechanical behavior. Considering now the low deformation regime (inset), the modulus is not affected and the yield stress is only slightly modified by increasing the fraction of loop chains. It is remarkable that all loop systems are confined between 0% loop and 20% cilia. Consequently, it appears that changing all chains from tie to loop chain affects mechanically the system less than cutting of 20% of TMs.

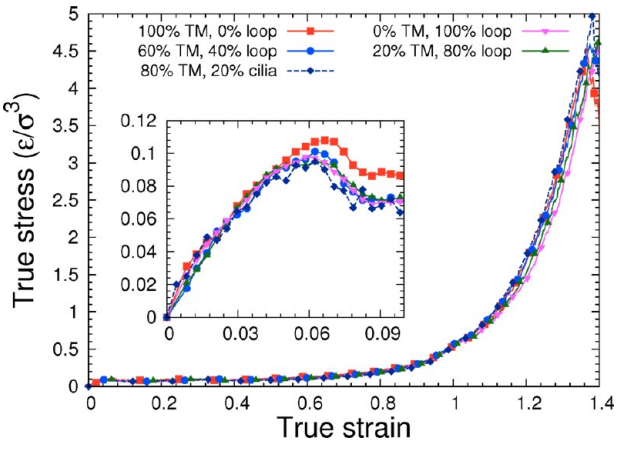

Figure 9. Mechanical response of different samples with various amounts of loop chains. The inset shows a zoom in the elastic regime and yield point region.

The most natural reason to explain this behavior is to evoke the possibility for the loop chains to form a definitive node in the rubbery phase. Two loop chains would then be equivalent to two TMs. The Primitive Path Algorithm[34] is the classical tool that is used in MD simulation to verify the presence of entanglements. A PPA algorithm has been modified to restrict its use only in the rubbery phase in order to check whether the chains are entangled or not.

In Figure 10, a 100% loop system is represented before and after its treatment by the PPA algorithm. It has been shown that nearly all the loop chains cannot separate from those coming from the opposite hard block. Actually, less than 20 chains over 320 are not entangled. This analysis confirms the hypothesis presented above..

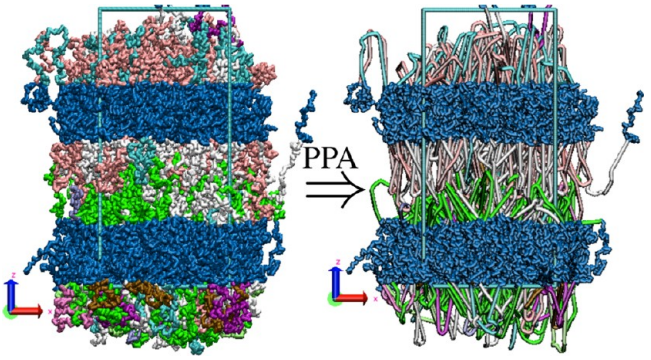

Figure 10. Primitive path of the rubbery chains portion in a triblock sample with 100% loop chains. Chains are unwrapped over the periodic boundary conditions of the simulation box. The loop chains are well entangled in a way that bridges the hard blocks together (knotted loop).

The entanglement rate that appear on Figure 10 could be seen as particularly high, knowing that chain length in the soft phase is 100 and entanglement length is generally admitted to be close to 70−80. However, in real systems, the phase separation step occurring during solvent evaporation or cooling down, leads to

dx.doi.org/10.1021/ma301286y | *Macromolecules* XXXX, XXX, XXX−XXX

the creation of chain loop and therefore, enforces the creation of entangled loops. Similarly, during our sample generation, chains grow in a confined space of thickness ≈20 σ. The size of each chain is 100 and the size of the random coil is slightly higher than 10 σ. Chains are growing simultaneously from each side of the lamella so that they naturally entangle in the middle. In a real sample, during demixing, the formation of loop chains leads to a non equilibrium situation where the two chain ends are confined in a specific area, presumably favoring entanglements of chains in the rubbery phase.

CONCLUSION

The aim of this paper was to validate (or invalidate) some physical ideas, present in the literature, concerning the role of molecular topology on mechanical behavior of layer block copolymers. Naturally, coarse-grained molecular dynamics is based on several hypothesis (bead−spring models, relatively short chains, unbreakable covalent bonds) that oversimplify what occurs in real materials. Moreover, the chain length in the rubbery phase is not significantly higher than the entanglement length, emphasizing the effect of tie and entangled loop molecules vs entangled cilia chains. However, it has been shown for high deformation that, TMs and entangled loop molecules essentially drive the mechanical behavior of the material.

However, qualitatively the results presented in this paper confirm many ideas present in the literature concerning the role of tie molecules (TMs) on the mechanical properties of nanostructured polymers. Increasing the amount of TMs will

- improve the resistance to cavitation
- decrease the plastic instability (stress drop at yield)
- improve the resistance to damage of the hard phase by chain pull-out

Semiquantitatively, it has been shown in particular that the strain hardening modulus increases linearly with the fraction of tie molecules until saturation occurs at approximatively 60%. The progressive destabilization of the interface may explain the latter result.

Finally, the role of loop molecules has been proved to be almost the same as that of tie molecules. A large majority of loop molecules are indeed entangled: two entangled loop chains are then equivalent to two tie molecules.

AUTHOR INFORMATION

Corresponding Author

*E-mail: olivier.lame@insa-lyon.fr.

Notes

The authors declare no competing financial interest.

ACKNOWLEDGMENTS

Computational support was provided by the Federation Lyonnaise de Calcul Haute Performance and GENCI/CINES . The financial support from ANR project Nanomeca is acknowledged. Part of the simulations were carried out using the LAMMPS molecular dynamics software (http://lammps.sandia.gov).

REFERENCES

(1) Kennedy, M. A.; Peacock, A. J.; Mandelkern, L. *Macromolecules* **1994**, *27*, 529−531.
(2) Popli, R.; Mandelkern, L. *J. Polym. Sci., Part B: Polym. Phys.* **1987**, *25*, 441−483.
(3) X. Lu, R. Q.; Brown, N. *Polymer* **1995**, *36*, 4239−4244.
(4) Kazmierczak, T.; Galeski, A.; Argon, A. *Polymer* **2005**, *46*, 8926−8936.
(5) Young, R. *Philos. Mag.* **1974**, *30*, 85−94.
(6) Crist, B.; Fisher, C.; Howard, P. *Macromolecules* **1989**, *22*, 1709−1718.
(7) Brooks, N.; Ghazali, M.; Duckett, R.; Unwin, A.; Ward, I. *Polymer* **1999**, *40*, 821−825.
(8) Brooks, N.; Mukhtar, M. *Polymer* **2000**, *41*, 1475−1480.
(9) Boyd, R. H. *J. Polym. Sci. Polym. Phys.* **1983**, *21*, 493−504.
(10) Oleinik, E. F. *Polym. Sci. Series C* **2003**, *45*, 17−117.
(11) Humbert, S.; Lame, O.; Seguela, R.; Vigier, G. *Polymer* **2011**, *52*, 4899−4909.
(12) Graham, J. T.; Alamo, R. G.; Mandelkern, L. *J. Polym. Sci., Polym. Phys.* **1997**, *35*, 213−223.
(13) Seguela, R. *J. Polym. Sci., Part B: Polym. Phys.* **2005**, *43*, 1729−1748.
(14) Humbert, S.; Lame, O.; Vigier, G. Ph.D. Thesis, INSA de Lyon, 2009.
(15) Nitta, K.; Takayanagi, M. *J. Polym. Sci., Part B: Polym. Phys.* **1999**, *37*, 357−368.
(16) Bonten, C.; Schmachtenberg, E. *Polym. Eng. Sci.* **2001**, *41*, 475−483.
(17) Seguela, R. *Macromol. Mater. Eng.* **2007**, *292*, 235−244.
(18) Bartczak, Z. *Macromolecules* **2005**, *38*, 7702−7713.
(19) Haward, R. *Macromolecules* **1993**, *26*, 5860−5869.
(20) Mori, Y.; Lim, L.; Bates, F. *Macromolecules* **2003**, *36*, 9879−9888.
(21) Sides, S. W.; Grest, G. S.; Stevens, M. J.; Plimpton, S. J. *J. Polym. Sci., Part B: Polym. Phys.* **2004**, *42*, 54−55.
(22) Monasse, B.; Queyroy, S.; Lhost, O. *Int. J. Mater Form-Springer/ESAFORM* **2008**, 949−986.
(23) Lee, S.; Rutledge, G. C. *Macromolecules* **2011**, *44*, 3096−3108.
(24) Kremer, K.; Grest, G. *J. Chem. Phys.* **1990**, *92*, 5057−5086.
(25) Auhl, R.; Everaers, R.; Grest, G.; Kremer, K.; Plimpton, S. *J. Chem. Phys.* **2003**, *119*, 12718−12728.
(26) Perez, M.; Lame, O.; Leonforte, F.; Barrat, J. *J. Chem. Phys.* **2008**, *128*, 234904.
(27) Pierce, F.; Perahia, D.; Grest, G. S. *EPL* **2011**, *95*, 46001.
(28) Makke, A.; Perez, M.; Lame, O.; Barrat, J. *J. Chem. Phys.* **2009**, *131*, 014904.
(29) Humbert, S.; Lame, O.; Chenal, J.; Rochas, C.; Vigier, G. *Macromolecules* **2010**, *43*, 7212−7221.
(30) Crist, B.; Metaxas, C. *J. Polym. Sci., Part B: Polym. Phys.* **2004**, *42*, 2081−2091.
(31) Bartczak, Z. *Macromolecules* **2005**, *38*, 7702−7713.
(32) Treolar, L. R. G. *J. Polym. Sci., Polym. Symp.* **1974**, *48*, 107−123.
(33) Humbert, S.; Lame, O.; Vigier, G. *Polymer* **2009**, *50*, 3755−3761.
(34) Sukumaran, S.; Grest, G.; Kremer, K.; Everaers, R. *J. Polym. Sci., Part B: Polym. Phys.* **2005**, *43*, 917933.